Infrared Optical Constants of Highly Diluted Sulfuric Acid Solution Droplets at Cirrus Temperatures

Robert Wagner,* Stefan Benz, Helmut Bunz, Ottmar Möhler, Harald Saathoff, Martin Schnaiter, and Thomas Leisner

Forschungszentrum Karlsruhe, Institute of Meteorology and Climate Research (IMK-AAF), Karlsruhe, Germany

Volker Ebert

University of Heidelberg, Physical Chemistry Institute, Heidelberg, Germany

Received: July 25, 2008; Revised Manuscript Received: September 11, 2008

Complex refractive indices for supercooled sulfuric acid solution droplets in the mid-infrared spectral regime (wavenumber range 6000−800 cm^{-1}) have been retrieved for acid concentrations ranging from 33 to 10 wt % H_2SO_4 at temperatures between 235 and 230 K, from 36 to 15 wt % H_2SO_4 at temperatures between 225 and 219 K, and from 37 to 20 wt % H_2SO_4 at temperatures between 211 and 205 K. The optical constants were derived with a Mie inversion technique from measured H_2SO_4/H_2O aerosol extinction spectra that were recorded during controlled expansion cooling experiments in the large coolable aerosol chamber AIDA of Forschungszentrum Karlsruhe. The new data sets cover a range of atmospherically relevant temperatures and compositions in the binary sulfuric acid/water system for which infrared refractive indices have not been published so far, namely, the regime when supercooled H_2SO_4/H_2O solution droplets at $T < 235$ K are subjected to an environment that is supersaturated with respect to the ice phase. With increasing ice supersaturation, the H_2SO_4/H_2O aerosol particles will continuously dilute by the uptake of water vapor from the gas phase until freezing of the solution droplets eventually occurs when the acid concentration has dropped below a critical, temperature-dependent threshold value. With the aid of the new measurements, the homogeneous freezing process of supercooled H_2SO_4/H_2O solution droplets at cirrus temperatures can be quantitatively analyzed by means of Fourier transform infrared spectroscopy, thereby overcoming a major drawback from previous studies: the need to use complex refractive indices that were measured at temperatures well above 235 K to deduce the composition of the low-concentrated H_2SO_4/H_2O aerosol particles. As in the case of the complex refractive indices for sulfuric acid solutions with acid concentrations greater than 37 wt % H_2SO_4, the new low-temperature optical constants for highly diluted droplets also reveal significant temperature-induced spectral variations in comparison with the refractive indices for higher temperatures, which are associated with a change in the equilibrium between sulfate and bisulfate ions.

1. Introduction

The homogeneous freezing of supercooled H_2SO_4/H_2O solution droplets is one important pathway in the formation of cirrus clouds in the upper troposphere.[1,2] In the laboratory, this low-temperature phase transition can be monitored with a variety of different techniques, including differential scanning calorimetry of emulsions[3] and the observation of freezing droplets using an optical microscope.[4] In addition, Fourier transform infrared (FTIR) spectroscopy is a well-suited method to study the composition and phase transition of submicrometer sized sulfuric acid aerosols, based on the distinct spectral changes in the frequency regime of the O−H stretching mode which occur when solid ice crystals nucleate from supercooled aqueous droplets.[5−7] Its quantitative applicability in terms of deriving the composition of the sulfuric acid solution droplets, however, relies on accurate frequency-dependent optical constants, i.e., the real and imaginary parts of the complex refractive index.

During the past decade, the database of optical constants in the binary sulfuric acid/water system has considerably improved, in particular owing to several studies of the strong temperature-induced changes in the dissociation behavior of H_2SO_4 in supercooled H_2SO_4/H_2O solution droplets, which leads to a strong variation of the optical constants in the sulfate absorption regime with temperature.[8−13] Optical constants for sulfuric acid below the homogeneous freezing temperature of pure water droplets (235 K) are now available from the studies by Tisdale et al.[10] for acid concentrations down to 45 wt % H_2SO_4, from Niedziela et al.[8] for compositions down to 32 wt % H_2SO_4, from Biermann et al.[11] for concentrations down to 30 wt % H_2SO_4, and from Myhre et al.[9] for compositions down to 38 wt % H_2SO_4. This compilation, however, still does not cover the composition range where the freezing of sulfuric acid droplets actually initiates at cirrus temperatures, namely at compositions ranging from about 25 to 7 wt % H_2SO_4 for temperatures between 190 and 230 K, based on the results of the droplet freezing experiments from Koop et al.[4] (see Table 1 therein).

Different groups have investigated the freezing of sulfuric acid aerosols in low-temperature flow-tube experiments by using FTIR extinction spectroscopy to derive the aerosol composition.[5−7] Bertram et al.[6] had to employ a calibration curve for the ratio of the hydroxyl and sulfate band areas in the infrared spectra calculated from room-temperature optical constants to deduce the acid concentration. Their measured freezing temperatures

* Corresponding author. E-mail: Robert.Wagner@imk.fzk.de.

10.1021/jp8066102 CCC: $40.75
Published on Web 10/23/2008

as a function of sulfuric acid droplet composition are systematically higher than those from the optical microscope study by Koop et al.,[4] a setup that presumably is less error-prone in terms of determining the accurate droplet composition. Cziczo and Abbatt[7] derived a calibration curve for the area ratio of a condensed-phase sulfate spectral feature to that of a condensed-phase water feature for temperatures above 253 K and assume that it also holds for temperatures between 234 and 200 K. Their derived ice freezing temperatures are lower than the optical microscope data from Koop et al.[4] Finally, Prenni et al.[5] obtained composition-dependent freezing temperatures for sulfuric acid aerosols that closely agree with the Koop et al.[4] results. Note that Prenni et al.[5] used an ice-coated conditioning chamber to set the aerosol composition to a fixed acid concentration, which then is supposed to remain unchanged in the observation region due to a high ratio of condensed-phase water relative to that in the gas phase. Hence, in this study FTIR spectroscopy was only applied to infer the onset of ice nucleation but not to derive the corresponding aerosol composition.

The significant scatter in the freezing temperatures for supercooled H_2SO_4/H_2O solution droplets from the different FTIR experiments might at least partially be explained by an inaccurate determination of the H_2SO_4 concentration of the aerosol particles, thereby underlining the need for accurate optical constants in the regime of low temperatures and low acid concentrations. In the compilation of freezing temperatures for different aqueous solutions by Koop et al.[14] (see Figure 1 therein), results from FTIR aerosol measurements were even completely omitted due to the assumption that these data might be subject to large uncertainties in composition. With our present work, we want to provide accurate infrared optical constants for the derivation of the composition and mass concentration of highly diluted sulfuric acid aerosols at cirrus temperatures.

A carefully designed experimental strategy is needed to deduce the low-temperature optical constants for sulfuric acid concentrations below 30 wt % H_2SO_4. In the bulk study by Biermann et al.,[11] such low acid concentrations were not accessible for temperatures below 233 K due to crystallization of the sample. Regarding measurements on airborne particles, the supercooled sulfuric acid droplets have to be exposed to an environment that is supersaturated with respect to ice to induce a dilution to such low acid concentrations; i.e., the actual water vapor pressure must be higher than the vapor pressure over ice at the given temperature. Furthermore, it must be assured that the aerosol particles have sufficient time to reach equilibrium with temperature and water vapor to possess a well-defined composition. Highly accurate water vapor measurements are then needed to infer the actual acid concentration using the Aerosol Inorganics Model (AIM, http://www.aim.env.uea.ac.uk/aim/aim.php),[15] supplemented by measurements of the aerosol mass loading to properly scale the simultaneously recorded infrared extinction spectra and to deduce the optical constants. We will outline in this paper that all these prerequisites are met when performing slow expansion cooling experiments in the large coolable aerosol chamber AIDA of Forschungszentrum Karlsruhe.[16] The experimental trajectory of such an expansion closely follows an atmospheric composition trajectory; i.e., initially concentrated sulfuric acid droplets are subjected to a gradually increasing relative humidity upon cooling. Thereby, the H_2SO_4/H_2O droplets continuously dilute until they finally freeze at some threshold composition. We have performed expansion experiments with initial AIDA gas temperatures of 235, 225, and 211 K and have deduced the mid-infrared optical constants (wavenumber range 6000−800 cm^{-1}) for sulfuric acid

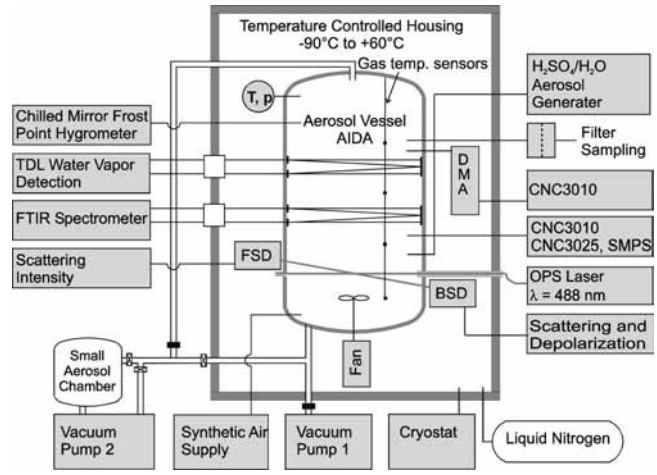

Figure 1. Schematic view of the AIDA aerosol chamber facility, featuring the relevant instrumentation for the sulfuric acid expansion cooling experiments.

in the composition range from 33 to 10 wt % H_2SO_4 at temperatures between 235 and 230 K, from 36 to 15 wt % H_2SO_4 at temperatures between 225 and 219 K, and from 37 to 20 wt % H_2SO_4 at temperatures between 211 and 205 K.

Our paper is organized as follows: In section 2, we will briefly review the general methodology of the AIDA expansion experiments and the chamber instrumentation before addressing in detail the expansion runs with the supercooled sulfuric acid droplets (section 3). Three main subsections will describe (i) the results from supplementary model calculations to confirm that the aerosol particles will remain in equilibrium with the changing temperature and relative humidity during the expansion coolings, (ii) our complementary approaches to accurately derive the composition of the H_2SO_4/H_2O droplets during the expansion cooling experiments, and (iii) the iterative method to derive the optical constants from the simultaneously recorded infrared extinction spectra. Our so-deduced data sets of optical constants will then be presented and discussed in section 4.

2. Experimental Section

A schematic cross section of the AIDA aerosol chamber facility, featuring the major scientific instrumentation used for the sulfuric acid expansion experiments, is shown in Figure 1.

The AIDA facility consists of a 84 m^3 sized, evacuable aluminum aerosol vessel inside an isolating containment whose interior can be cooled to temperatures as low as 183 K.[16,17] A mixing fan, located at the bottom of the aluminum vessel, is continuously operating during the expansion experiments and reduces the temperature inhomogeneities throughout the mixed part of the gas volume to ±0.2 K, as monitored by arrays of horizontally and vertically arranged temperature sensors. With a horizontal line of five temperature sensors mounted close to the aluminum walls of the AIDA chamber, we have measured a thickness of less than 10 cm for the transition layer between the vertical vessel walls and the mixed part of the gas volume. In addition, the operation of the mixing fan provides for homogeneous conditions in terms of the water partial pressure as well as the aerosol and cloud particle number concentration and size throughout the chamber volume.[18] Prior to an expansion cooling cycle, the following preparation steps have to be carried out: (i) Evacuation of the chamber to <0.1 hPa, followed by flushing cycles with particle-free synthetic air to establish background particle concentrations of less than 0.1 cm^{-3}. (ii) Refilling the chamber with humidified synthetic air to 1000 hPa

at a higher temperature (typically about 268 K) and subsequent cooling to the temperature, which was chosen as the starting temperature for the freezing experiment. Upon cooling, the excess water vapor forms a thin ice layer on the chamber walls, meaning that an expansion cycle is started at an ice saturation ratio $S_{ice} = p_w(T)/p_{w,ice}(T)$ close to 1: the water vapor partial pressure, $p_w(T)$, is roughly equal to the saturation pressure over ice, $p_{w,ice}(T)$. (iii) Addition and characterization of the sulfuric acid solution droplets, as described in detail below.

To initiate the freezing of the sulfuric acid droplets, the AIDA pressure is reduced by controlled pumping, typically with pumping rates between 50 and 100 L min^{-1}, leading to maximum cooling rates of about 0.5 K min^{-1}. During pumping, p_w decreases at most linearly with the total pressure (implying a constant water vapor mixing ratio) whereas $p_{w,ice}$ decreases exponentially with the gas temperature. Thereby, ice supersaturated conditions with S_{ice} well above 1.6 can be established inside the chamber. The humidification rate dS_{ice}/dt during expansion cooling is further enhanced by evaporation of ice from the chamber walls because the wall temperature remains almost constant. This tends to restore the partial pressure p_w in the chamber to the initial value before the pumping was started. In the limiting case of an ultrafast evaporation of water vapor from the ice-coated chamber walls, the water partial pressure would remain constant. The true time evolution of p_w during pumping, measured by direct tunable diode laser absorption spectroscopy, usually lies between these two extremes.[19] The sulfuric acid solution droplets continuously dilute in the course of the expansion cooling experiment by the uptake of water vapor from the gas phase until the acid concentration drops below a temperature-dependent threshold value where droplet freezing occurs. Expansions were started at a reduced pumping speed to ensure that the initial humidification rate dS_{ice}/dt was less than 0.07 min^{-1}. Later on, the pumping speed was increased to maintain a reasonable humidification rate. As proved by the complementary model calculations presented in section 3, the major part of the volume size distribution of the sulfuric acid droplets had sufficient time to maintain equilibrium with the gas phase while the temperature and water vapor pressure changed during pumping. The overall duration of an expansion cooling cycle from the start of pumping to the onset of freezing was typically between 800 and 1200 s. In the following, we will briefly outline the relevant instruments and the numerical model which are used for the analysis of the sulfuric acid freezing experiments.

Aerosol Generation and Characterization. The sulfuric acid solution droplets were generated by passing synthetic air (2.5−4.0 L min^{-1}) with a water content of about 1 ppm over 96 wt % sulfuric acid at 135−145 °C. Supercooled droplets of aqueous sulfuric acid are formed by binary nucleation of sulfuric acid and water when the sulfuric acid/air mixture is cooled in the stainless steel connection tube between the heated saturator and the cooled AIDA chamber. By modulating the flow speed of the synthetic air and the temperature of the saturator, H_2SO_4/H_2O solution droplets of different sizes could be generated. The size distributions, measured with a low temperature and pressure differential mobility particle sizer (DMA) connected to a condensation particle counter (CNC3010, TSI), closely mimicked log-normal distributions. As discussed in section 3, the aerosol generator was tuned to produce sulfuric acid droplets with count median diameters preferentially in the range 0.4−0.5 μm. Note that the DMA system is operated at almost the same temperature and pressure as the AIDA chamber.[20] For each starting temperature of our freezing experiments, we conducted at least two independent expansion cooling cycles to check the reproducibility of the retrieved optical constants. The aerosol number concentrations of the 0.4−0.5 μm-sized droplets were about 10000−25000 cm^{-3}, individually adjusted for each experiment to obtain a high signal-to-noise ratio in the infrared extinction spectra.

Total aerosol sulfate mass concentrations were measured by ion chromatographic analysis of nylon filter samples as described in detail elsewhere.[21] Note that both the size distribution and the filter measurements are techniques that are only applicable to characterize the sulfuric acid droplets before the start of an expansion cooling cycle. During pumping, the time resolution of these techniques is too slow to monitor the rapidly changing H_2SO_4/H_2O droplet sizes and the sulfuric acid mass loading.

Selective Gas-Phase Water Measurements. Fast and highly accurate water vapor measurements can be used in combination with the AIM model to quantitatively deduce the composition of the sulfuric acid solution droplets during the expansion cooling cycles. In our setup, we used direct tunable diode laser absorption spectroscopy dTDLAS[22] to derive precise absolute water vapor mixing ratios[23] from the spectrally resolved, narrowband absorption losses of laser radiation sent through the AIDA chamber. A horizontally oriented, fiber-coupled, open-path White-type multiple reflection absorption cell,[24,25] which is directly mounted at mid height onto the inside walls of the aerosol vessel (see Figure 3a in Wagner et al.[18]), defined the absorption path length (23.6 m path length at higher and 68.9 m at lower concentrations), which was selected to optimize the signal-to-noise ratio of the spectrometer. A fiber-coupled, room-temperature, near-infrared telecom-type diode laser module with internal optical isolator and up to 10 mW output power was used to access the (000 → 101) (110 → 211) gas-phase water absorption line at 7299.43 cm^{-1} (1369.97 nm) in the H_2O $\nu_1 + \nu_3$ combination and $2\nu_1$ overtone band. This line was chosen for minimized spectral interference and temperature sensitivity using a new line selection software[26] and carefully characterized with respect to its line strength (error ±3%), pressure broadening coefficient (±0.2%), and its respective temperature coefficient N (±1.5%)[27] over the 200−300 K range. By continuous laser wavelength scanning via rapid triangular modulation (139.8 Hz) of the diode laser current, the almost complete absorption line profile was captured, averaged, and analyzed with a nonlinear Levenberg−Marquardt fitting algorithm using a multiline fit with Voigt line shapes. The data evaluation procedure, previously developed for open-path TDLAS measurements in combustion processes,[28] water sprays,[29] and on stratospheric balloon platforms,[30] ensured a precise correction of the broadband optical scattering losses caused by the aerosol and cloud particles along the absorption path, as well as the pressure and temperature changes during the expansion. This permitted a precise measurement of the integrated line area, which was then converted into water vapor mixing ratios using the ideal gas law and the measured pressures (±0.1 hPa) and temperatures (±0.2 K) inside the aerosol vessel. We achieved with 1.5 s temporal resolution a concentration resolution of about 30−300 ppb depending on the absorption path length and the disturbance levels caused by particle scattering. The absolute accuracy, which was recently investigated in an international water vapor instrument intercomparison campaign AQUAVIT,[31] is estimated to be ±3−5% and dominated by the line strength uncertainty of ±3%.[25,27]

In addition to the interstitial water vapor which is measured with the TDL setup, the total water concentration (i.e., including water contained in the sulfuric acid solution droplets) is

measured with a fast high-precision chilled mirror hygrometer (MBW, model 373 LX). The instrument is located outside the thermostated housing of the chamber and samples pass through a heated (30 °C) stainless steel tube to ensure complete evaporation of the water droplets. Consequently, the difference between the MBW and TDL data directly gives the water content of the sulfuric acid solution droplets. Provided that it represents a significant fraction of the total water concentration, this quantity in combination with the sulfuric acid mass concentration data is a complementary gauge of the solution droplet composition during the expansion cycle.

In Situ FTIR Extinction Measurements. A FTIR spectrometer (type IFS 66v, Bruker) is coupled to one of the White cells at level two of the AIDA chamber to record infrared extinction spectra of the sulfuric acid solution droplets in the chamber. The infrared white cell is equipped with BaF_2 cell windows, their transmittance confining the measurements to the 6000−800 cm^{-1} spectral range. During an expansion cooling cycle, the infrared spectra are typically recorded at a rate of 6 spectra min^{-1} with 4 cm^{-1} resolution. Due to the low humidification rates dS_{ice}/dt during the expansion cooling experiments the acid concentration decreases by less than 0.25 wt % H_2SO_4 in the course of a single FTIR measurement. This deviation is well below the overall uncertainty in the determination of the acid concentration (±2 wt % H_2SO_4; see section 3) and is therefore neglected. Depending on the starting temperature of the expansion cooling cycle, the optical path length of the White cell was adjusted between 106 and 227 m. At higher temperatures, a reduced optical path length is indispensable to avoid saturation of the infrared beam due to the intense absorption lines of gas-phase water. A comprehensive description of the experimental setup of the FTIR system can be found in Wagner et al.[18]

In Situ Laser Light Scattering and Depolarization Measurements. At level one of the AIDA chamber, the laser beam of an optically pumped semiconductor (OPS) laser (emission at 488 nm, >100:1 vertical polarization) is directed horizontally through the AIDA chamber and is dumped in a beam trap at the opposite chamber wall. The polarization plane of the incident laser light can be aligned parallel or perpendicular to the scattering plane using a liquid crystal polarization rotator. The horizontal scattering plane is defined by the light beam and the overlapping detection apertures of two telescope optics that probe scattered light from the center of the chamber in near forward direction (scattering angle 2°) and polarization-resolved in near backward direction (scattering angle 178°). A Glan-Laser polarization prism with two exit windows is used to split the back-scattered light into the parallel and perpendicular components with respect to the initial polarization plane. Forward-scattered light and the two polarization components in backscattering direction are detected by three independent photomultiplier tubes operating in the photon counting mode with 1 s integration time. With I^{for}, I^{back}_{par} and I^{back}_{per} denoting the background-corrected scattering intensities measured in the three channels, we define the scattering ratio ρ and the linear depolarization ratio δ as $\rho = (I^{for})/(I^{back}_{par} + I^{back}_{per})$ and $\delta = (I^{back}_{per})/(I^{back}_{par})$, respectively.

The scattering measurements are a valuable tool to study both the condensational growth of sulfuric acid solution droplets and the subsequent freezing event. With the onset of pumping, the mass growth of the H_2SO_4/H_2O aerosol particles leads to an increase in the scattering intensities in the forward and parallel-polarized backward channels that can be quantitatively analyzed with Mie scattering calculations to determine the size of the swelling droplets and thus the amount of the water uptake. The phase transition from spherical solution droplets to aspherical ice crystals can be readily detected by the sharp increase in the depolarization ratio δ.

Model Calculations of the Condensational Growth of the Sulfuric Acid Solution Droplets. If the vapor pressure of H_2O above the aqueous sulfuric acid solution droplets differs from its partial pressure in the surrounding gas phase, water molecules are transported by diffusion to (condensation) or from (evaporation) the particles. The mass flux is proportional to the difference between the partial pressure of the condensing gas and its vapor pressure at the particle surface, which is a function not only of temperature but also of particle composition and size. In the computer model MAID[32] applied in this study, the particle size distribution is approximated by a number of discrete size bins so that size as well as composition effects can be taken into account in a realistic way. To calculate the actual mass growth rate of the H_2SO_4/H_2O solution droplets by the water uptake during the expansion cycles, the formulation of Dahneke[33] is implemented;

$$\frac{dm}{dt}(t,r,m_W,m_{SA}) = 4\pi r D\beta(c_\infty - c_{sur}(T,r,m_W,m_{SA}))$$

$$\beta = \frac{Kn_D + 1}{2Kn_D(Kn_D + 1)/\alpha + 1} \qquad Kn_D = \frac{2D}{\langle v \rangle r} \quad (1)$$

with $(dm)/(dt)(t,r,m_W,m_{SA})$, mass growth rate; $m_{W,SA}$, mass fraction of water and sulfuric acid; t, time; r, radius; c, H_2O concentration far away (∞) and on the particle surface (sur); T, temperature; D, diffusion coefficient of H_2O; Kn_D, Knudsen number, $\langle v \rangle$, mean molecular velocity; and α, mass accommodation coefficient.

The term β depends mainly on the particle size and the mass accommodation coefficient and takes into account noncontinuum effects that are important mainly for submicron particles. Whereas for large particles (>1 μm) the transport is dominated by the diffusion field, for smaller particles the transport approaches the free-molecule regime and accommodation effects become important. For the particle sizes in our experiments, it can be expected that the accommodation gets important if α is below 0.1,[34] but measurements of α show that it is in the order of 0.5 for the condensation of H_2O on electrolytic solutions.[35]

Important issues that can be quantitatively analyzed by the model runs are on the one hand the impact of the Kelvin effect on the composition of small particles, and on the other, the kinetic growth limitation for large particles in cases where the humidification rate dS_{ice}/dt is fast in comparison with the condensation rate. In the first case the sulfuric acid concentration in the droplets has to be higher in comparison with the equilibrium value to compensate the Kelvin effect. In the case of larger droplets the water activity may differ significantly from the equilibrium value unless there is enough time for the particle growth. But as can be seen from eq 1, the mass growth rate scales with r and the relative growth rate (the inverse of the characteristic time of condensation) with r^{-2}. Therefore, depending on particle size and rate of change of the saturation level, the water fraction and the corresponding water activity of the droplets lags behind the equilibrium value. Together with the Kelvin effect for small particles, this kinetic effect may provoke that during the expansion experiments, the actual H_2SO_4/H_2O aerosol composition becomes strongly dependent on the size of the droplets if the pumping speed is chosen too high so that the water activity of the larger particles will not approach the equilibrium.

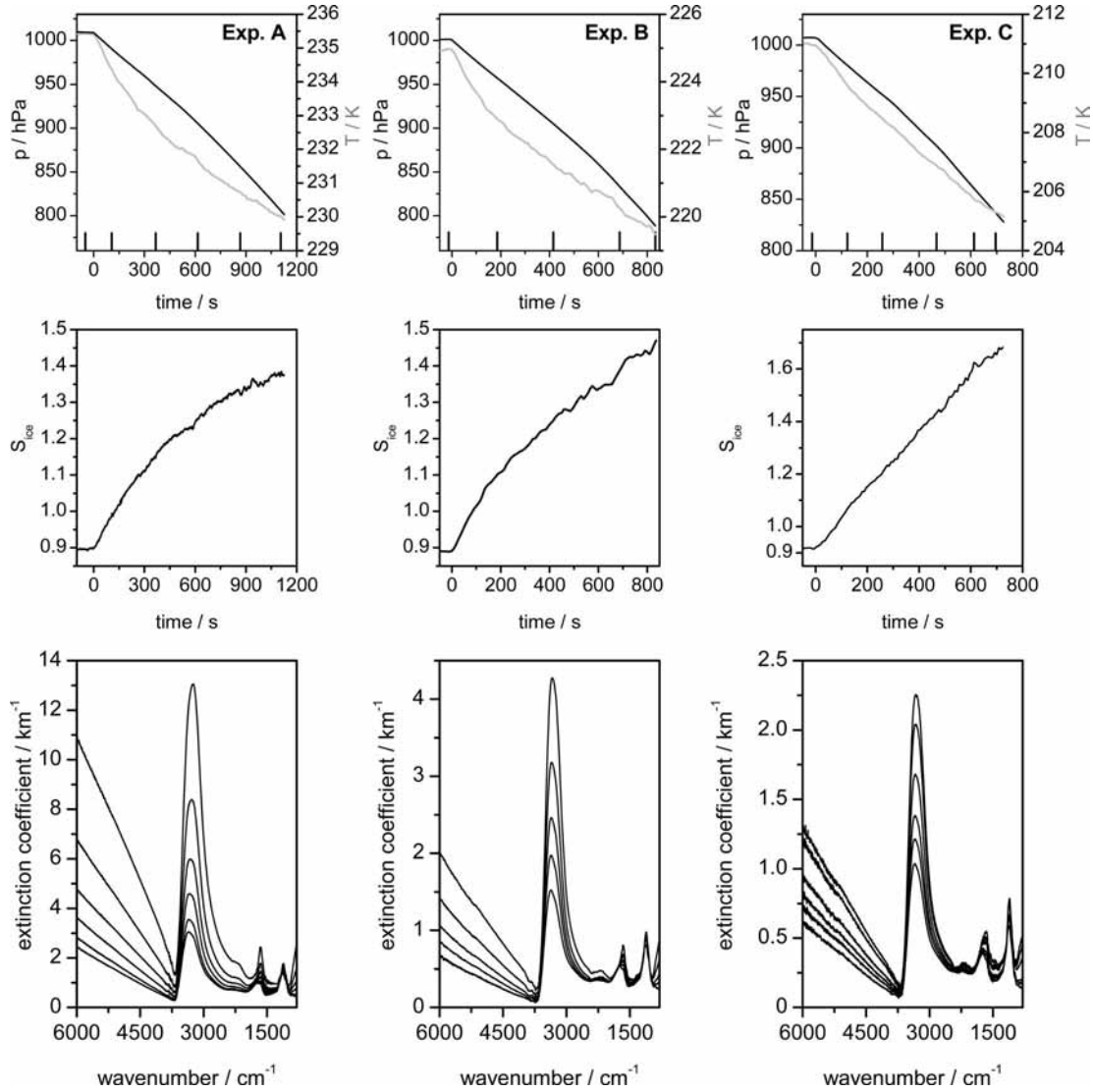

Figure 2. Top row panels: time series of AIDA pressure (black lines) and mean AIDA gas temperature (gray lines) for three different expansion cooling cycles with supercooled sulfuric acid solution droplets. Middle row panels: time evolution of the saturation ratio with respect to ice (S_{ice}) during pumping. Bottom row panels: FTIR extinction spectra recorded at different times during the expansion cycles, as marked by the vertical bars on the time scales in the top row panels. Absorption lines due to gas-phase water have been subtracted. Note that the pumping speed was increased in the course of each expansion to stabilize the humidification rate.

3. Analysis of the H_2SO_4/H_2O Aerosol Freezing Experiments

General Overview. In Figure 2, we have compiled time series of the various AIDA data for three expansion cooling experiments with supercooled sulfuric acid solution droplets which were started at gas temperatures of 235 K (exp **A**), 225 K (exp **B**), and 211 K (exp **C**). The top row panels show the time evolution of the pressure and the mean gas temperature in the aerosol vessel. The latter represents the average value of an array of four vertically oriented thermocouple sensors, as shown in Figure 1. In the second row panels, we show the time-dependent saturation ratios with respect to ice, obtained as quotients of the measured water vapor pressures (TDL measurements) and the vapor pressures over ice at the given temperatures.[36] The time axis spans the regime from the start of pumping (time zero) until the freezing onset of the sulfuric acid solution droplets, i.e., the time when an increase in the depolarization ratio indicated the formation of aspherical ice crystals. Finally, the bottom row panels depict series of infrared extinction spectra that were recorded in the course of the expansion cooling cycles. The individual times for the spectra recordings are denoted by the small vertical bars on the time scales of the top row panels. With respect to their temporal order, the spectra are to be read from bottom to top; i.e., the lowermost extinction spectrum in each panel represents the concentrated sulfuric acid solution droplets prior to pumping, whereas the uppermost spectrum is characteristic of the diluted droplets immediately before the first spectral signatures of the nucleated ice crystals could be detected. The continuous dilution of the sulfuric acid aerosol during pumping is nicely indicated by the successive increase of the intensity of the broad extinction band around 3300 cm^{-1} which is attributable to the O−H stretching mode of liquid water. In addition, the growth of the solution droplets by the water uptake from the gas phase is reflected in the strong increase of the scattering intensity at nonabsorbing wavenumbers above 3700 cm^{-1}. Note that the relative amount of water uptake during the expansion cycles decreases with decreasing gas temperature; i.e., the freezing of the H_2SO_4/H_2O solution droplets at lower temperatures already initiates at higher acid concentrations.

The spectra series shown in the bottom panels of Figure 2 are the underlying data in our present study. To quantitatively

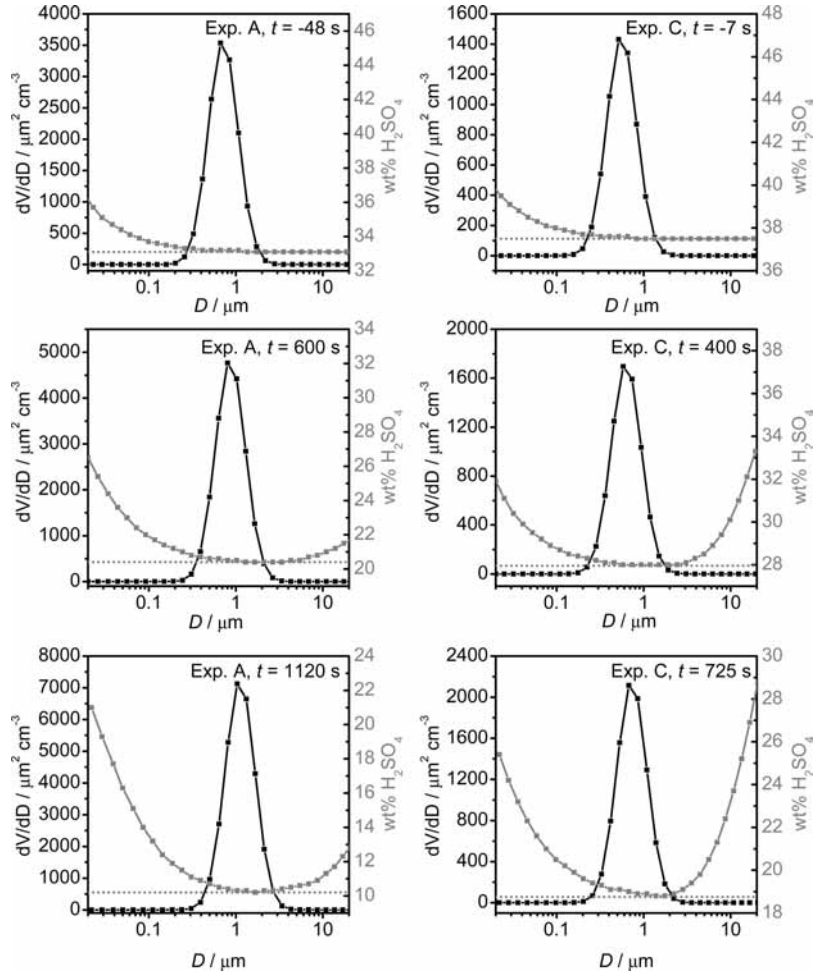

Figure 3. H_2SO_4/H_2O aerosol volume size distributions (black lines) and size-resolved chemical compositions (solid gray lines) for three time steps during the expansion cooling experiments **A** and **C** from Figure 2, as calculated with the aerosol model MAID. The dotted gray horizontal lines denote the equilibrium composition of H_2SO_4/H_2O for the prevailing water vapor pressure in the case of a flat surface.

retrieve the infrared optical constants for the variously concentrated sulfuric acid droplets from the measured spectra, we have to determine for each time step of the spectra recordings the following two quantities: (i) the size distribution parameters of the sulfuric acid solution droplets, needed as input values in our inverse Mie approach to deduce the optical constants, and (ii) the composition of the H_2SO_4/H_2O aerosol particles during pumping. In particular, we have to clarify that each spectrum indeed reflects an aerosol of uniform composition: The condensational growth of the sulfuric acid aerosol particles must be so fast that those droplets that belong to the large-diameter tail of the size distribution (and thus represent a significant fraction of the overall aerosol mass concentration) also have sufficient time to adjust to the increasing relative humidity and thereby feature the same composition as droplets of smaller sizes.

Model Results for the Condensational Growth of the H_2SO_4/H_2O Solution Droplets. The aerosol size distributions and size-resolved chemical compositions during the expansion cycles were calculated with the computer model MAID as described in section 2. The simulations were constrained by prescribing the initial aerosol size distribution and the measured time series of temperature, pressure, and gas-phase water concentration. Exemplary model results for the size-resolved sulfuric acid mass fractions of the solution droplets during pumping are compiled in Figure 3: For the expansion experiments **A** and **C** from Figure 2, the modeled size-resolved droplet compositions are shown together with the concomitant aerosol volume size distributions at three different time steps: before the start of pumping (top row), in the middle of the expansion cycle (middle row), and immediately before the freezing onset (bottom row).

Before the start of pumping, the sulfuric acid mass fraction in the aerosol particles only depends on the particle size due to the Kelvin effect. The Kelvin term notably enhances the water vapor pressure over sulfuric acid for particle diameters below about 0.2 μm, thus leading to a higher acid concentration on the small-diameter tail of the size distribution. During the expansion experiments, also larger droplets with diameters greater than about 2 μm begin to deviate from the equilibrium composition because the humidification rate, albeit deliberately reduced by employing low pumping speeds in the expansion cycles, is still faster than the condensation rate of water for such large droplet sizes. This kinetic effect is more pronounced in experiment **C**, as can be explained by the lower absolute water vapor concentration and the reduced diffusion coefficient at the lower temperature. In addition, the Kelvin effect gets more prominent in the course of the expansion cycles compared to the static conditions before the pumping was started. At t = 1120 s during experiment **A**, for example, only sulfuric acid droplets of diameters between 0.8 and 2 μm hold the equilibrium acid concentration for a flat surface. Already for droplets with diameters below 0.8 μm, the Kelvin term leads to a significant increase in the acid concentration in comparison with the

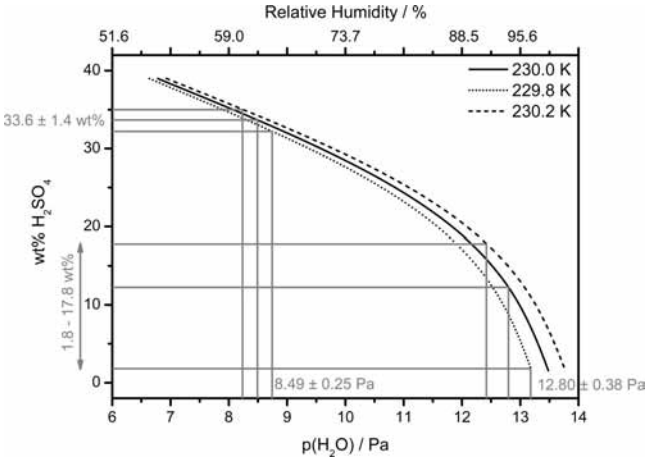

Figure 4. Equilibrium vapor pressure of H_2O above aqueous H_2SO_4 as a function of the acid concentration at temperatures of 229.8, 230.0, and 230.2 K, as calculated with the AIM model. The top axis denotes the relative humidity with respect to supercooled water for the 230.0 K computation. The gray lines denote numerical examples to assess the uncertainty of the droplet composition which is associated with uncertainties in the water vapor pressure and the temperature (see text for details).

equilibrium composition. So, for the less concentrated sulfuric acid droplets (acid concentration about 10 wt % H_2SO_4 at t = 1120 s), a higher increase in the acid concentration in relation to the equilibrium value is needed to compensate for the same relative increase in the water vapor pressure due to the Kelvin effect than is necessary for the more concentrated aerosol particles before the start of the expansion (33 wt % H_2SO_4 at t = −48 for experiment **A**). This is because the slope of the curve that relates the equilibrium water vapor pressure to the acid concentration (wt % H_2SO_4 as a function of p_w) gets steeper toward lower acid concentrations. This effect will be addressed again in the following subsection in the context of Figure 4 and has already been observed in former model calculations of the AIDA expansion experiments; see Figure 9 in Haag et al.[37]

The particle sizes for which the droplet compositions significantly deviate from the equilibrium value, however, only contribute to a minor part to the overall aerosol volume concentration. As for experiment **A** at t = 1120 s, for example, all droplets in the size range from D = 0.5−6.9 μm deviate by less than 0.5 wt % H_2SO_4 from the equilibrium composition for a flat surface. But those sulfuric acid droplets represent 99.1% of the overall aerosol volume concentration. In this way, we have confirmed by the supplementary model calculations that for the entire duration of all our expansion cycles more than 98% of the total aerosol volume concentrations were contributed by droplets which differed by less than 0.5 wt % from the equilibrium composition. This criterion is guaranteed as the best, provided that the median droplet diameters of the H_2SO_4/H_2O number size distributions at the start of the expansion are approximately in the range from 0.4 to 0.5 μm. This optimum droplet size is, on the one hand, large enough so that the Kelvin effect becomes negligible but, on the other hand, so small that the kinetic effect of a delayed condensational droplet growth is still insignificant.

Droplet Composition in the Course of the Expansion Cycles. The results from the model calculations have underlined that the infrared spectra can be analyzed to a very good approximation by adopting a size-independent droplet composition at each time step during the expansion cycles that is equal to the equilibrium composition for the prevailing water vapor concentration. In principle, the model output would deliver all quantities that we considered as necessary input values for the retrieval procedure of the optical constants, i.e., time-resolved size distributions and droplet compositions. But the accuracy of these values crucially depends on the quality of the water vapor measurements, as we want to underline with the following numerical example. In Figure 4, we have calculated with the aid of the AIM model the saturation water vapor pressure over aqueous sulfuric acid as a function of the acid concentration at a temperature of 230.0 ± 0.2 K. For high acid concentrations in the regime around 35 wt % H_2SO_4, representing the droplet composition before the start of the expansion experiments, the droplet composition changes only slightly as function of the equilibrium water vapor pressure. A 3% uncertainty in the water vapor measurements (numerical example: 8.49 ± 0.25 Pa) in combination with a temperature uncertainty of ±0.2 K would transform into an error of less than 1.5 wt % H_2SO_4 in the droplet composition (33.6 ± 1.4 wt % H_2SO_4). For more diluted droplets, however, the same uncertainties in the water vapor and temperature measurements would transform into a much larger uncertainty in the aerosol composition, because the slope of the wt % H_2SO_4−$p(H_2O)$ curve strongly increases when approaching 100% relative humidity with respect to supercooled water. For example, a measured water vapor pressure of 12.80 ± 0.38 Pa at a gas temperature of 230 ± 0.2 K would only constrain the droplet composition to the broad range of 1.8−17.8 wt % H_2SO_4.

In addition, we have not considered so far the absolute accuracy of calculating the equilibrium water vapor pressure over sulfuric acid from thermodynamic data with the AIM model. A comparison between measured partial pressures of H_2O over aqueous sulfuric acid with those calculated from thermodynamic data also revealed deviations in the order of a few percent (see Figure 9 in Massucci et al.[38]). These considerations make clear that the combined uncertainties of the TDL water vapor measurements and the AIM model predictions may result in large uncertainties of the inferred H_2SO_4/H_2O droplet composition during the expansion cycles, especially at higher temperatures where the droplets dilute to low acid concentrations until freezing occurs. We therefore propose two further strategies to derive the droplet composition, both based on the analysis of the FTIR extinction spectra.

At first glance, it might appear surprising just to use the FTIR spectra to derive the aerosol composition in view of the lack of accurate optical constants which we have stressed so far. But both methods explore the relative spectral changes in reference to the extinction spectrum of the H_2SO_4/H_2O solution droplets before the start of the expansion where the composition, size distribution, and mass concentration of the aerosol particles are accurately known. These spectral changes are then transferred into changes in the aerosol properties relative to those before the start of pumping.

Before describing the FTIR analyses, we want to underline that we can rely on different supplementary methods to accurately characterize the injected sulfuric acid aerosol particles before the start of pumping, choosing experiment **C** from Figure 2 as an example: Before the start of the expansion, we have measured a water vapor pressure of 0.736 ± 0.022 Pa at T = 211.0 ± 0.2 K; see Figure 7, bottom panel. With the aid of the AIM model, this translates into an equilibrium acid concentration of 37.4 ± 1.2 wt % H_2SO_4. The ion chromatographic analysis of a nylon filter sample yielded a H_2SO_4 mass concentration of 440 $\mu g/m^3$. From these data we can infer a condensed-water mass concentration of 736 $\mu g/m^3$, or, expressed as a water partial

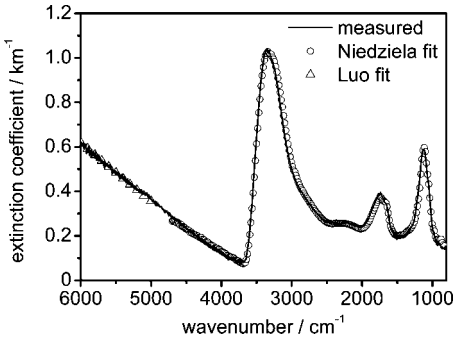

Figure 5. Measured infrared extinction spectrum at $t = -13$ during expansion experiment **C** shown in Figure 2 (black line) in comparison with two Mie-calculated extinction spectra for a log-normal H_2SO_4/H_2O aerosol number size distribution with $N = 12000$ cm^{-3}, $\sigma_g = 1.493$, and CMD = 0.41 μm. The open circle trace was computed with the optical constants by Niedziela et al.[8] for an acid concentration of 36 wt % H_2SO_4 at 210 K. The second calculation (triangles) was done with the refractive indices obtained from the Luo et al.[39] model for 37.4 wt % H_2SO_4 at 211 K.

pressure at 211 K, of 0.072 Pa. This value can be validated by a comparison with the difference between the total water concentration measured with the MBW frost point hygrometer (0.809 Pa at $t < 0$; see Figure 7) and the TDL gas-phase water concentration (0.736 Pa): This yields an aerosol water content of 0.073 Pa, in close agreement with the value above. Additionally, for the more concentrated H_2SO_4/H_2O solution droplets, there are literature data for the infrared optical constants with which we can analyze the extinction spectrum of the aerosol particles at $t < 0$. Figure 5 shows the Mie-calculated infrared extinction spectrum of sulfuric acid for a log-normal aerosol number size distribution with $N = 12000$ cm^{-3}, σ_g (mode width) = 1.493, and CMD (count median diameter) = 0.41 μm (open circles) in comparison with the spectrum measured at $t = -13$ s (solid line). For the Mie computation, we employed the optical constants for 36 wt % H_2SO_4 at 210 K from Niedziela et al.[8] (derived by an interpolation of the 32 and 39 wt % H_2SO_4 data sets). For this acid concentration, we obtained the best agreement between the Mie calculation and our measured spectrum. The size distribution parameters were taken from the CNC and DMA measurements. The value for the count median diameter originally derived from the log-normal fit to the DMA measurement had to be slightly increased (<10%) so that the integrated volume size distribution of the solution droplets, multiplied with the H_2SO_4/H_2O density (eq A10 in Carslaw et al.[15]) and the acid concentration, exactly yielded the H_2SO_4 mass concentration from the nylon filter analysis. The latter technique has proved in a former study as an accurate reference method for the determination of H_2SO_4 aerosol mass loadings.[21] The underestimation of the H_2SO_4 mass concentration in the DMA measurements is most presumably related to the fact that synthetic air with a frost point temperature of about 205−210 K is used as sheath air in the DMA setup. Therefore, in particular during experiments **A** and **B**, the H_2SO_4/H_2O solution droplets will partially evaporate when entering the DMA system. Although operating at chamber temperature and pressure, the DMA setup does not exactly reproduce the relative humidity of the chamber interior.

The calculated extinction spectrum accurately fits the measured spectrum, taking into account that also for the literature data set of optical constants an uncertainty in the acid concentration of at least ±1 wt % H_2SO_4 has to be considered. A further robust test for the accuracy of the size distribution data is demonstrated with the second Mie-fit shown in Figure 5 (triangle trace). Here, we have used the real refractive indexes from the model by Luo et al.[39] to calculate the extinction spectrum of sulfuric acid at nonabsorbing wavenumbers between 6000 and 5000 cm^{-1} for an acid concentration of 37.4 wt % and $T = 211$ K. The model by Luo et al.[39] has been refined by new measurements of the refractive indices in the $H_2SO_4/HNO_3/H_2O$ system at stratospheric temperatures[40] and should therefore deliver the most accurate available optical data to check the accuracy of the input parameters for the H_2SO_4/H_2O aerosol size distribution. Indeed, with the prescribed size distribution parameters, the measured spectrum is accurately matched between 6000 and 5000 cm^{-1}.

A Mie-fitting procedure in this spectral regime with accurately known, composition- and temperature-dependent refractive index data can also be considered as the most exact technique to derive the composition and size distribution of the sulfuric acid aerosol particles during the expansion cycles. Thus, we quantitatively relate the continuous increase in the scattering signal between 6000 and 5000 cm^{-1} during pumping (see bottom panels in Figure 2) to the condensational growth of the H_2SO_4/H_2O solution droplets: Let us denote the initial size distribution parameters of the sulfuric acid droplets at $t = 0$ with N_0, $\sigma_{g,0}$, and CMD_0. At a given time t during the expansion cycle, the aerosol number concentration can be calculated, taking into account the dilution due to pumping, according to $N_t = N_0(p_t/p_0)(T_0/T_t)$. As we have shown by the model calculations, all droplet sizes that significantly contribute to the overall aerosol volume concentration undergo the same relative increase in diameter during pumping; therefore, the mode width should not change, $\sigma_{g,t} = \sigma_{g,0}$. From the TDL water vapor measurements in combination with the AIM model, we are able to obtain an initial guess for the composition of the H_2SO_4/H_2O solution droplets at time t for which we calculate the refractive indices between 6000 and 5000 cm^{-1} with the Luo et al.[39] model. These refractive index data are then used as input values in a Mie-fitting procedure to retrieve the count median diameter of the sulfuric acid solution droplets at time t by minimizing the summed-square residuals between measured and calculated extinction spectrum, using CMD_t as the only optimization parameter. With the so-derived CMD_t value, we can calculate the overall aerosol volume concentration, and, after multiplication with the aerosol density (using eq A10 from Carslaw et al.[15] with the initial guess for the H_2SO_4/H_2O composition), the overall aerosol mass concentration, $m_{H_2SO_4/H_2O,t}$. In the same way as the aerosol number concentration, the sulfuric acid mass concentration will decrease during pumping according to $m_{H_2SO_4,t} = m_{H_2SO_4,0}(p_t/p_0)(T_0/T_t)$, with $m_{H_2SO_4,0}$ derived from the filter analysis. With wt % $H_2SO_{4,t} = 100 \cdot m_{H_2SO_4,t}/m_{H_2SO_4/H_2O,t}$, we thereby obtain a new value for the acid concentration at time t that will replace the initial guess composition in a further iteration to get a refined result for CMD_t. The iterative procedure is continued until the relative difference in CMD_t between two successive iterations is less than 0.1%. Usually, convergence is obtained after only one or two iterations because the initial guess of the aerosol composition is already quite accurate and both the H_2SO_4/H_2O density and the refractive indices between 6000 and 5000 cm^{-1} weakly depend on small changes in the acid concentration.

The basic idea of the second approach to deduce the H_2SO_4/H_2O composition from the IR spectra is to use the integrated intensity of the broad O−H stretching mode around 3300 cm^{-1} as a quantitative measure of the condensed-water mass concentration, $m_{H_2O,t}$, during pumping. The band integral can be calibrated with the accurately known liquid water content at t

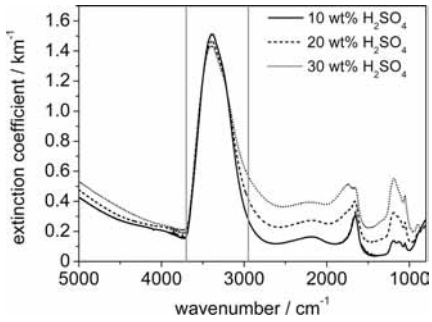

Figure 6. Mie-calculated infrared extinction spectra of log-normally distributed supercooled sulfuric acid solution droplets at $T = 263$ K using the optical constants from Biermann et al.[11] for acid concentrations of 10, 20, and 30 wt % H_2SO_4. The employed size distribution parameters are $N = 10000$ cm^{-3}, $\sigma_g = 1.45$, CMD $= 0.5$ μm for 10 wt % H_2SO_4; $N = 10500$ cm^{-3}, $\sigma_g = 1.45$, CMD $= 0.5$ μm for 20 wt % H_2SO_4; and $N = 11210$ cm^{-3}, $\sigma_g = 1.45$, CMD $= 0.5$ μm for 30 wt % H_2SO_4. The adjustments of the aerosol number concentrations ensure that all size distributions yield a common condensed-water mass concentration of 1181 μg/m^3. The calculated spectra were analyzed by integrating the O−H stretching extinction band between 3700 and 2950 cm^{-1}, as indicated by the vertical gray bars; the band integrals for the three spectra are 0.567 cm^{-2} (10 wt % H_2SO_4), 0.559 cm^{-2} (20 wt % H_2SO_4), and 0.563 cm^{-2} (30 wt % H_2SO_4).

$= 0$, i.e., $\int$OH-band$_0 = m_{H_2O,0}$. From the band integral obtained at a given time t during pumping, the acid concentration can then be calculated according to

$$\text{wt \% } H_2SO_{4,t} = 100 \cdot \frac{m_{H_2SO_4,t}}{m_{H_2SO_4,t} + m_{H_2O,t}}$$

$$m_{H_2SO_4,t} = m_{H_2SO_4,0}(p_t/p_0)(T_0/T_t)$$

$$m_{H_2O,t} = m_{H_2O,0}\frac{\int \text{OH-band}_t}{\int \text{OH-band}_0} \quad (2)$$

This method will only be reliable if the spectral features of liquid water within the regime of the O−H stretching mode are not significantly influenced by the decreasing acid concentration of the solution droplets during pumping. Figure 6 depicts the results of test calculations with the H_2SO_4/H_2O optical constants from Biermann et al.[11] for acid concentrations of 30, 20, and 10 wt % H_2SO_4 at 263 K. The latter represents the minimum temperature for which the optical constants of the highly diluted sulfuric acid solutions are available. We have computed the infrared extinction spectra for the three acid concentrations for log-normal number size distributions with identical mode width and count median diameter ($\sigma_g = 1.45$, CMD $= 0.5$ μm) but where the aerosol number concentration was individually adjusted so that the liquid water mass concentration is the same for all three calculations ($m_{H_2O} = 1181$ μg/m^3).

With decreasing acid concentration, the O−H stretching band gradually gets narrower, concomitantly leading to a higher value for the peak extinction coefficient. But we can define an integration range from 3700 to 2950 cm^{-1} for which the integrated band intensities are almost the same for all three acid concentrations. Note that the extinction coefficient at 3700 cm^{-1} is used as the base point for the integration. Thus, independent of the acid concentration, the integration over this wavenumber range can be used to scale $m_{H_2O,t}$ in relation to $m_{H_2O,0}$ throughout the expansion cycle. As a minor drawback of this method, the integration result is not completely independent of particle size.

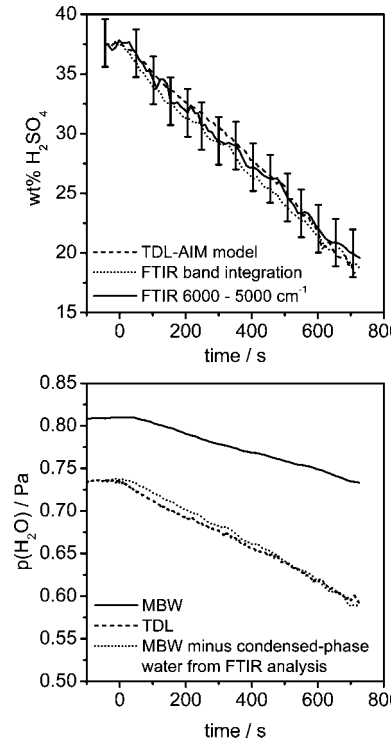

Figure 7. Top panel: composition of the supercooled sulfuric acid solution droplets in the course of expansion experiment **C** shown in Figure 2. The acid concentration was derived from three independent analyses; see text for details. Bottom panel: time series of independent water measurements during experiment **C**: (i) total water content measured with the MBW frost point hygrometer (solid line), (ii) gas-phase water content measured with the TDL spectrometer (dashed line), and (iii) difference between the MBW measurement and the condensed-water content derived from the FTIR composition analysis based on the spectral fit in the 6000−5000 cm^{-1} regime (dotted line).

The magnitude of the 3700−2950 cm^{-1} band integral is not entirely related to volume-dependent light absorption but also contains a smaller size-dependent contribution due to light scattering. The latter portion will increase during the expansion cycle as a result of the condensational growth of the sulfuric acid droplets, thereby leading to a potential overestimation of the liquid water mass concentration. For small particles with size parameters x ($x = \pi D/\lambda$)[41] below 1, the scattering contribution could be approximated with sufficient accuracy by a λ^{-4} wavelength dependency and subtracted from the extinction spectrum prior to the integration; see, for example, Figure 4 in Norman et al.[42] For median particle diameters of up to 0.8 μm (size parameter $x = 1$ at 4000 cm^{-1}), however, the scattering cross sections already reveal a pronounced dispersion feature within the O−H vibrational resonance which cannot be reproduced by the λ^{-4} behavior. To assess the influence of the increasing scattering contribution to the 3700−2950 cm^{-1} band integral, we have made the following test calculations. The relative increase in the median droplet diameters during pumping ranges from a factor of about 1.3 for Exp. **C** (final droplet composition prior to freezing about 20 wt % H_2SO_4) to 1.6 for exp **A** (final droplet composition about 10 wt % H_2SO_4). We have therefore computed two further extinction spectra with the Biermann et al.[11] optical constants using the following parameters: (i) $N = 4780$ cm^{-3}, $\sigma_g = 1.45$, CMD $= 0.65$ μm for 20 wt % H_2SO_4 and (ii) $N = 2442$ cm^{-3}, $\sigma_g = 1.45$, CMD $= 0.8$ μm for 10 wt % H_2SO_4. Again, in both calculations, the aerosol number concentration was adjusted to yield the same liquid

water content as in the computation for 30 wt % H_2SO_4 with $\sigma_g = 1.45$ and CMD = 0.5 μm. The obtained 3700−2950 cm^{-1} band integrals are 0.563, 0.596, and 0.639 cm^{-2} for the computations with 30, 20, and 10 wt % H_2SO_4, respectively. Thus, the maximum overestimation of $m_{H_2O,t}$ in the course of the different expansion experiments, owing to the increasing scattering contribution to the O−H stretching band integral, will be on the order of 6% if the aerosol particles would only dilute to 20 wt % H_2SO_4 during the expansion and about 13% if the sulfuric acid droplets would dilute to 10 wt % H_2SO_4. According to eq 2, this results in a maximum underestimation of the acid concentration of about 1 wt % H_2SO_4. Obviously, the absolute accuracy of the band integration method crucially depends on the assumption that the relative spectral changes in the O−H stretching regime for low acid concentrations of 10−30 wt % H_2SO_4 are comparable between the temperature of 263 K and the lower temperatures at which our experiments were actually conducted. We therefore consider this method as a supplement to the evidently more accurate aerosol composition analysis using the Mie fit to the 6000−5000 cm^{-1} spectral regime.

In the top panel of Figure 7, we show a comparison between the three independent methods to derive the H_2SO_4/H_2O aerosol composition during the expansion cycles for experiment **C**: (i) the combination of the TDL gas-phase water measurement and the AIM model, (ii) the infrared method based on the integration of the O−H stretching mode extinction band, and (iii) the FTIR method relying on the spectral fit to the 6000−5000 cm^{-1} regime. The agreement between the three approaches is excellent. The spread in the obtained acid concentrations, as indicated by the error bars, is well below ±2 wt % H_2SO_4, which we thus consider as an upper limit for the uncertainty of the H_2SO_4/H_2O composition analysis. The high accuracy and the self-consistency of the water measurements for this experiment are further evidenced by the lower panel of Figure 7. Here, it is demonstrated that the direct measurement of the gas-phase water concentration with the TDL spectrometer closely corresponds to the difference of the total water content measured with the MBW frost point hygrometer and the condensed-water content deduced from the FTIR approach using the 6000−5000 cm^{-1} spectral fit. An equally good agreement between the individual methods for the H_2SO_4/H_2O composition analysis was also observed for experiment **B**, whereas the data for experiment **A**, shown in Figure 8, need closer inspection. Both approaches based on the infrared spectra analysis again show a close agreement of the H_2SO_4/H_2O composition during pumping. The band integration method tends to yield slightly lower acid concentrations at later times during the experiment, which might be explained by the increased scattering contribution to the O−H band integral in the course of the expansion, thereby leading to an overestimation of the droplet dilution. The composition results from the TDL-AIM model analysis, however, do not reproduce the FTIR findings as well as in experiments **B** and **C**, in particular in the final period of the expansion where the droplets have become highly dilute. Similarly, the difference between the measured total water and FTIR-deduced condensed water content does not exactly reproduce the directly measured gas-phase water concentration. Note that the relative deviation between these two curves is not larger than 3%, it just reflects the combined experimental uncertainties, including, for example, the uncertainty in the temperature-dependent line strength of the water vapor absorption line which is used in the TDL analysis and the frost point temperature error of the MBW humidity measurements. When applying the combined TDL-AIM model approach, these small uncertainties in the water

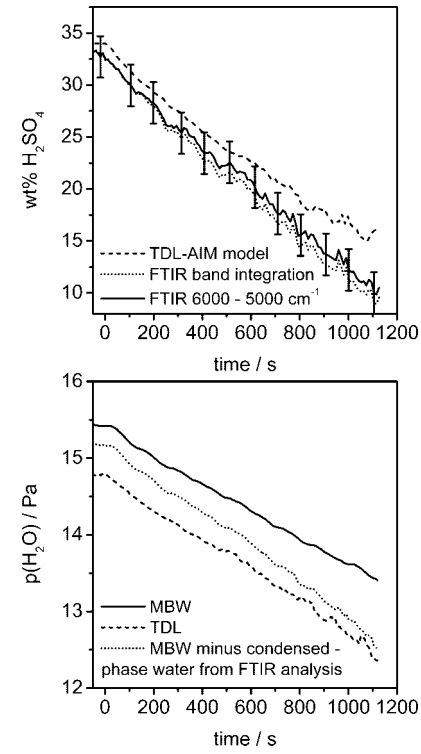

Figure 8. Top panel: composition of the supercooled sulfuric acid solution droplets in the course of expansion experiment **A** shown in Figure 2. The acid concentration was derived from three independent analyses; see text for details. Bottom panel: time series of independent water measurements during experiment **A**: (i) total water content measured with the MBW frost point hygrometer (solid line), (ii) gas-phase water content measured with the TDL spectrometer (dashed line), and (iii) difference between the MBW measurement and the condensed-water content derived from the FTIR composition analysis based on the spectral fit in the 6000−5000 cm^{-1} regime (dotted line).

measurements translate into comparably large errors for the H_2SO_4/H_2O aerosol composition at low acid concentrations, as demonstrated by the numerical examples shown in Figure 4. We therefore attribute the discrepancy between the composition analysis with the TDL-AIM approach and the FTIR results during experiment **A** to either experimental uncertainties (line strength and/or temperature error) or potential inaccuracies of the AIM model-calculated saturation water vapor pressures for these particular acid concentrations and temperatures. For this reason we have computed the condensational growth of the sulfuric acid solution droplets during this expansion (left panel of Figure 3), by constraining the MAID model runs to the saturation water vapor pressures for the H_2SO_4/H_2O compositions obtained from the FTIR analysis rather than to the original TDL data.

The accuracy of the FTIR results for the H_2SO_4/H_2O aerosol composition during experiment **A** can be validated by our complementary scattering intensity measurements. In Figure 9, we show a comparison between the measured scattering intensity in near-forward direction in the course of the expansion and two traces calculated with Mie theory for the droplet size distributions deduced from (i) the FTIR composition analysis (spectral fit in the 6000−5000 cm^{-1} regime) and (ii) the combined TDL-AIM model approach. The real refractive index for the H_2SO_4/H_2O solutions droplets at the wavelength of 0.488 μm, required as input in the Mie scattering calculations, changes in time due to the successive dilution of the particles. The time-dependent

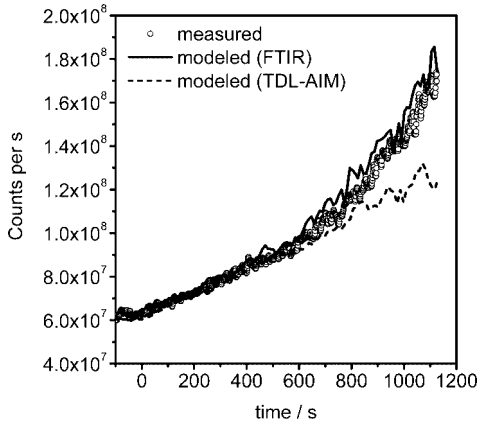

Figure 9. Measured forward-scattered intensity from the in situ laser light scattering measurements during expansion experiment **A** (dotted trace) in comparison with two time profiles calculated with Mie theory. The solid black line denotes the scattering intensities obtained when using the H_2SO_4/H_2O size distribution parameters from the FTIR analysis (6000−5000 cm^{-1} spectral fit) as input values in the Mie calculations; the dashed line represents the results for the computation with the size distribution parameters deduced from the combined TDL-AIM model approach. See text for details.

refractive indices were calculated with the Luo et al.[39] model, each with the current acid concentration and temperature as input values. When employing the FTIR-deduced size distribution parameters, the measured increase in the scattering intensity, induced by the continuous condensational growth of the solution droplets, is accurately reproduced. In the combined TDL-AIM model analysis, the droplets do not dilute as much as predicted by the FTIR results, in particular at later times during the expansion. This results in a smaller relative increase of the median H_2SO_4/H_2O droplet diameter during pumping which fails to reproduce the measured trace of the forward-scattering intensity. We will therefore use for all expansion experiments the time-resolved aerosol number size distributions and compositions deduced from the Mie-fits to the wavenumber regime from 6000 to 5000 cm^{-1} as input values for our iterative approach to deduce the mid-infrared H_2SO_4/H_2O optical constants, as described in the following section.

Iterative Approach to Derive the Optical Constants of H_2SO_4/H_2O. Our iterative approach to deduce the optical constants of the supercooled sulfuric acid solution droplets closely follows the procedure we have employed in a previous work to extract the infrared refractive indices of supercooled water.[43] The necessary input data for the retrieval of a specific n and k data set, with n and k denoting the real and imaginary part of the complex refractive index $N(\tilde{\nu}) = n(\tilde{\nu}) + ik(\tilde{\nu})$, are (i) the measured infrared extinction spectrum, (ii) the corresponding H_2SO_4/H_2O aerosol composition as well as the number concentration, mode width, and count median diameter of the log-normal number size distribution, and (iii) an initial guess for the k spectrum used as starting point in the iteration scheme. For the latter, we employed the imaginary indices for 32 wt % H_2SO_4 at $T = 210$ K from Niedziela et al.[8] With the initial guess optical constants we then computed with the aid of Mie theory the infrared extinction spectrum for the given aerosol size distribution and calculated the summed squared residuals between the measured and computed infrared spectrum. In the next step, this quantity was minimized by adjusting the optical constants which were employed in the Mie calculation, thereby retrieving an optimized refractive index data set for the given acid concentration and temperature.

In the minimization step, we used the complete k spectrum between 3748 and 800 wavenumbers as optimization parameters, summing up to 738 grid points for a spectral resolution of 4 cm^{-1}. The downhill simplex method was used as the optimization technique.[44] After obtaining a new guess for the k values between 3748 and 800 cm^{-1}, the wavenumber range of the k spectrum was extended to 6000 cm^{-1} by setting all k values equal to zero in the nonabsorbing 6000−3752 cm^{-1} regime. Thereafter, we calculated via the Kramers−Kronig transformation the corresponding spectrum of the real part of the refractive index, as outlined in detail in the following paragraph. With the new set of n and k, we recomputed the residuals between measured and calculated spectrum and continued this iteration scheme until convergence was obtained, meaning that the k values for the current iteration step deviated by less than 0.0005 from the previous one.

The subtractive Kramers−Kronig transformation was used to calculate the real refractive index n at any given wavenumber $\tilde{\nu}_0$ from the wavenumber-dependent k spectrum according to:

$$n(\tilde{\nu}_0) = n(\tilde{\nu}_x) + \frac{2(\tilde{\nu}_0^2 - \tilde{\nu}_x^2)}{\pi} P\int_0^\infty \frac{k(\tilde{\nu})\tilde{\nu}}{(\tilde{\nu}^2 - \tilde{\nu}_0^2)(\tilde{\nu}^2 - \tilde{\nu}_x^2)}\, d\tilde{\nu} \quad (3)$$

Here, $n(\tilde{\nu}_x)$ is the real refractive index at the so-called anchor point, denoting a frequency within the wavenumber range of the measurements where the value for n is accurately known. We computed this anchor point value for the measured H_2SO_4/H_2O composition and temperature with the Luo et al.[39] model at 5000 cm^{-1}. The numerical integration was performed using Maclaurin's formula method as described by Ohta and Ishida.[45] The subtractive Kramers−Kronig technique is supposed to reduce the uncertainties associated with the extension of the k spectrum beyond the spectral range which is covered by the measurements.[46,47] Here, approximations for the unknown habitus of the k spectrum have to be introduced. We chose to extend the k spectrum below our low-frequency cutoff of 800 cm^{-1} with the room-temperature H_2SO_4/H_2O optical constants from Palmer and Williams,[48] which are available for wavenumbers down to 400 cm^{-1}. The extension spectra were calculated for the actual H_2SO_4/H_2O composition by interpolating between the Palmer and Williams[48] data sets for 25 and 38 wt % H_2SO_4, and, for acid concentrations below 25 wt % H_2SO_4, by interpolating between the 25 wt % H_2SO_4 data set and the k spectrum for pure water at 298 K from Bertie and Lan.[49] The spectrum of pure water was then also employed as an extension of our measured spectra for wavenumbers between 400 and 12 cm^{-1}. The pure water spectrum was scaled by an offset to match the Palmer and Williams[48] extension spectra at 400 cm^{-1}, and the combined extension spectra were then scaled again to match the 6000−800 cm^{-1} k spectrum from our measurements at 800 cm^{-1}. To assess the effect of the low-frequency approximations of the k spectrum on the result of the subtractive Kramers−Kronig transformation, we have made a test calculation with the refractive index data set for 38 wt % H_2SO_4 at 213 K from Myhre et al.[9] This data set was obtained by combined measurements in the mid-infrared (down to a wavenumber of 400 cm^{-1}) and the far-infrared regime (down to 20 cm^{-1}), and, therefore, no approximations had to be introduced prior to the Kramers−Kronig transformation. We thus consider the n spectrum between 6000 and 800 cm^{-1} as a true reference spectrum. In Figure 10, this original spectrum for the real refractive index is compared to the n spectrum obtained after the Kramers−Kronig transformation of a modified k spectrum; i.e., the original k spectrum

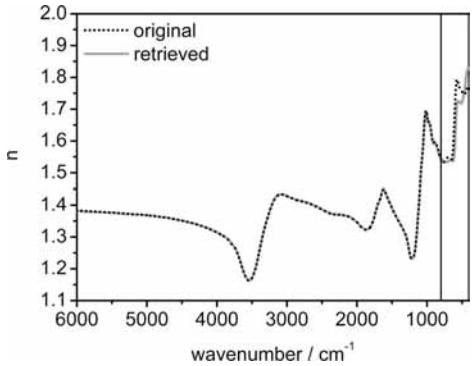

Figure 10. Quantitative test of the subtractive Kramers−Kronig transformation. Black dotted line: original spectrum of the real part of the refractive index from the data set for 38 wt % H_2SO_4 at 213 K from Myhre et al.[9] The gray spectrum was obtained by the subtractive Kramers−Kronig transformation of a combination of the following k spectra: 7500−800 cm^{-1}, original k spectrum for 38 wt % H_2SO_4 at 213 K from Myhre et al.;[9] 800−400 cm^{-1}, k spectrum for 38 wt % H_2SO_4 at 298 K from Palmer and Williams;[48] and 400−12 cm^{-1}, k spectrum for pure water at 298 K from Bertie and Lan.[49] An anchor point value of $n(\tilde{\nu}_x) = 1.3687$ at 5000 cm^{-1}, adopted from the original Myhre et al.[9] n spectrum, was employed in the integration. The vertical black line denotes the low-frequency cutoff of our measurements at 800 cm^{-1}.

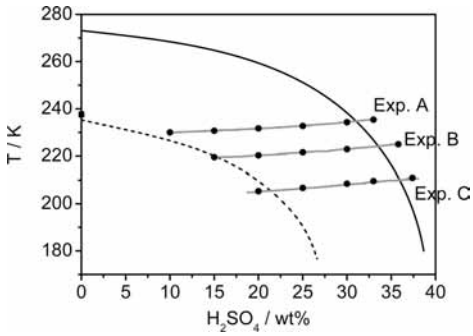

Figure 11. Experimental trajectories of the three expansion cooling experiments with supercooled sulfuric acid solution droplets from Figure 2 within the sulfuric acid−water phase diagram (gray traces). The acid concentrations were deduced with the 6000−5000 cm^{-1} Mie fitting procedure to the measured infrared spectra, as outlined in the previous section. Highlighted by black dots on the trajectories are the specific acid concentrations for which the H_2SO_4/H_2O optical constants were determined. The solid black line indicates the ice melting-point curve, whereas the dashed black line denotes the critical ice nucleation temperatures as a function of H_2SO_4/H_2O composition from the study by Koop et al.[4] (see Table 1 therein). The black square at $T = 238$ K and 0 wt % H_2SO_4 symbolizes a recent measurement of the optical constants for supercooled water.[43]

from Myhre et al.[9] was truncated at 800 cm^{-1} and extended with the Palmer and Williams[48] k spectrum for 38 wt % H_2SO_4 at 298 K and the pure water optical constants as described above. Obviously, the approximations introduced in the k spectrum for wavenumbers below 800 cm^{-1} only marginally influence the accuracy of the retrieved n spectrum in the spectral range of our measurements. Only for wavenumbers well below the low-frequency cutoff of our setup at 800 cm^{-1}, the Kramers−Kronig integration result for the modified k spectrum starts to deviate notably from the original n spectrum.

4. Results and Discussion

In Figure 11, we show the experimental trajectories of the three expansion cooling experiments from Figure 2 within the sulfuric acid−water phase diagram. The starting compositions of the initially concentrated supercooled sulfuric acid droplets are approximately given by the ice melting-point curve due to the ice-coating of the inner walls of the AIDA chamber. Due to some internal hot spots (mixing fan, heated sampling tubes, heating foils beneath the mirrors of the White-type reflection cells which prevent them from icing), the mean gas temperature is usually a few tenths of a Kelvin higher than the wall temperature at static conditions. Thereby, the chamber air is slightly subsaturated with respect to ice (ice saturation ratio about 0.9, see middle row panels of Figure 2) and the supercooled H_2SO_4/H_2O solution droplets are slightly more concentrated compared to the composition given by the ice melting-point curve for a specific temperature. The end points of the trajectories denote the H_2SO_4/H_2O aerosol composition just prior to freezing. It can be seen that our temperature-dependent data set for the H_2SO_4/H_2O aerosol freezing deviates to some extent from the results of the optical microscope study by Koop et al.,[4] an issue which will be addressed in detail in a separate manuscript.

In the present work, we have derived the infrared optical constants of the supercooled sulfuric acid solutions droplets for a set of different acid concentrations along the experimental trajectories shown in Figure 11. Selected results are displayed in Figure 12; the complete data sets are available as Supporting Information through the journal web page (see below).

The series of the k spectra reveal the expected spectral trends; i.e., within the sets of spectra obtained from either experiment **A** or experiment **C** (top and middle panels of Figure 12) the intensity of the O−H stretching mode gradually increases with decreasing H_2SO_4 content whereas the opposite trend is discernible in the regime of the absorption bands of the sulfate, SO_4^{2-}, and bisulfate, HSO_4^-, ions. When focusing on the relative spectral changes in the sulfate absorption regime for the data sets from experiment **A**, one notes that the absorption band of the most concentrated sample (33 wt % H_2SO_4) still reveals a distinct fine structure because the relative contributions of the sulfate and bisulfate ions to the overall absorption spectrum are similar in magnitude. The peak frequency is at about 1110 cm^{-1}, corresponding to the ν_3 SO_4^{2-} band, but the distinct shoulder at 1050 cm^{-1} and the smaller peak at 900 cm^{-1} denote a substantial contribution from the HSO_4^- ion (ν_1 and ν_4 band, respectively); see Querry et al.[50] for the band assignment. Upon dilution, the equilibrium progressively shifts toward the sulfate ion and the spectral features of the bisulfate ion become less pronounced. In addition, a new absorption band emerges at the low-frequency limit of our measurements, representing the high-frequency tail of the intense intermolecular rotational mode of liquid water centered at about 580 cm^{-1}.[50] The peak frequency of the O−H stretching band experiences a slight red shift when going to more dilute solution droplets. Following the explanation given by Niedziela et al.,[8] this trend can also be related to the equilibrium change from the singly charged bisulfate ion to the doubly charged sulfate ion: The so-induced strengthening of the ion−water solvent hydrogen bonding might explain the red-shift and increased intensity of the O−H vibrational band. In the k spectra series derived from experiment **A** we have added the k spectrum of pure supercooled water at $T = 238$ K for comparison;[43] the measurement is also symbolized by the square in Figure 11. This data set can be considered as a valuable anchor point to check the consistency and accuracy of the results for the deduced optical constants for experiment

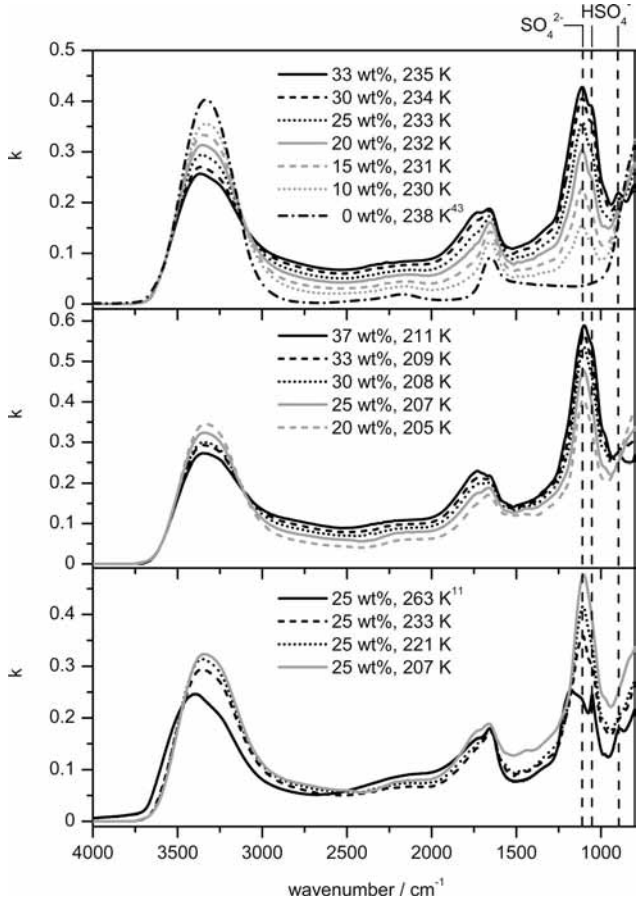

Figure 12. Spectra of the imaginary part of the complex refractive of H_2SO_4/H_2O for different acid concentrations (expressed as wt % H_2SO_4) and temperatures. Top panel: data sets retrieved from expansion experiment **A**; the *k* spectrum of pure water at 238 K from the study by Wagner et al.[43] is shown for comparison. Middle panel: data sets retrieved from expansion experiment **C**. Bottom panel: *k* spectrum of 25 wt % H_2SO_4/H_2O at 263 K from Biermann et al.[11] in comparison with the low-temperature data sets from the present study. The dashed vertical black lines denote the band assignment in the sulfate absorption regime.

A: Along the experimental trajectory, the optical constants for H_2SO_4/H_2O should gradually approach the pure water reference data. Indeed, when the relative spectral changes that are induced by a 10 wt % reduction in the acid concentration are inspected, i.e., the variations between the 30 and 20 wt % as well as between the 20 and 10 wt % H_2SO_4 data sets, the pure water spectrum adequately represents the spectral changes, which would be expected for the removal of the remaining acid contribution in the 10 wt % H_2SO_4 *k* spectrum.

As to the *k* data sets inferred from experiment **C**, the lower temperature provokes an additional shift of the bisulfate−sulfate equilibrium toward SO_4^{2-}. This implicates that already the *k* spectrum for the initial aerosol composition (37 wt % H_2SO_4) is dominated by the spectral features of the sulfate ion and the relative spectral changes in the fine structure of the sulfate absorption band upon dilution are less pronounced as for the data sets from experiment **A**. In the bottom panel of Figure 12, we show the temperature dependence of the *k* spectrum for a fixed acid concentration of 25 wt % H_2SO_4. Our low-temperature data sets are compared to the Biermann et al.[11] data set at 263 K. The strong spectral changes again underline the pronounced ion equilibrium shift toward the sulfate ion upon cooling, thus resembling the results for the temperature-dependency of the

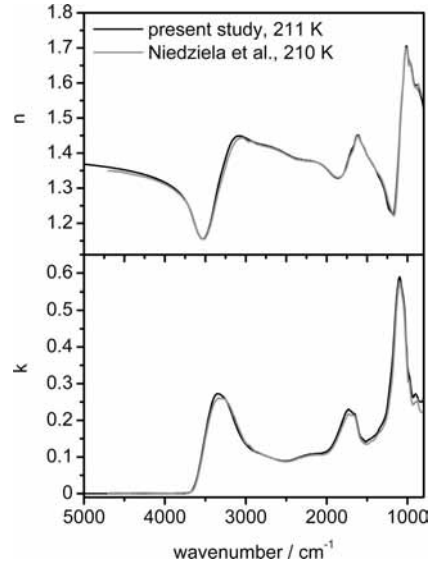

Figure 13. Spectra of the real and imaginary parts of the complex refractive index for aqueous sulfuric acid with 37 wt % H_2SO_4. Black lines represent the data sets from our present study; the corresponding values from the Niedziela et al.[8] database (interpolation of the 32 and 39 wt % H_2SO_4 data sets) are shown in gray.

H_2SO_4/H_2O optical constants which were already observed for higher acid concentrations.[8,9,11] Our data sets thus fill a gap in the as yet extensive but not entirely complete database of optical constants for the binary sulfuric acid/water system at atmospherically relevant temperatures and compositions: covering the regime when supercooled H_2SO_4/H_2O solutions droplets at $T < 235$ K start to dilute in an environment which has become supersaturated with respect to the ice phase until the droplet freezing initiates after the acid concentration has dropped below a critical, temperature-dependent threshold value.

The accuracy of the retrieved *n* and *k* data sets mainly depends on the accuracy of the measured H_2SO_4/H_2O mass concentration before the start of the expansion, because this value is used as the reference to which the increase in the aerosol mass loading during pumping is referred to. Any uncertainty in $m_{H_2SO_4/H_2O,0}$ will therefore directly propagate into the derived *n* and *k* spectra. We have therefore highlighted in the previous section that the accuracy of this quantity can be cross-checked by complementary measurement techniques. We only see two chances for a direct comparison of our retrieved *n* and *k* spectra with other literature data. First, as discussed above, the optical constants for pure water at 238 K represent a proper extension of the H_2SO_4/H_2O data sets derived along the trajectory of experiment **A**. Second, for the starting point of experiment **C**, we can compare our data set for 37 wt % H_2SO_4 at 211 K with the equivalent from the Niedziela et al.[8] database (Figure 13).

Both the infrared spectra of the real and the imaginary parts of the complex refractive index show a very good agreement. The maximum absolute deviation between the two *k* spectra, for example, does not exceed a value of 0.02; the maximum relative difference between the two *k* data sets in the peak regime of the O−H stretching mode is about 7%. Figure 14 demonstrates how a 5% change in the aerosol mass loading would affect the retrieval results for the *n* and *k* spectra. It includes a comparison between the *n* and *k* data sets for 20 wt % H_2SO_4 at 232 K which were derived (i) with the original set of size distribution parameters inferred from the FTIR analysis and (ii) with a modified parameter set where the aerosol number concentration was scaled by a

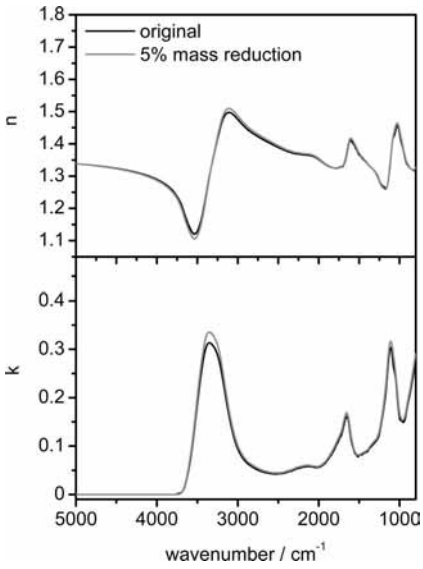

Figure 14. Spectra of the real and imaginary parts of the complex refractive index for aqueous sulfuric acid with 20 wt % H_2SO_4 at T = 232 K. Black lines represent the original data sets, and the spectra shown in gray were obtained for a 5% reduction in the aerosol mass concentration; see text for details.

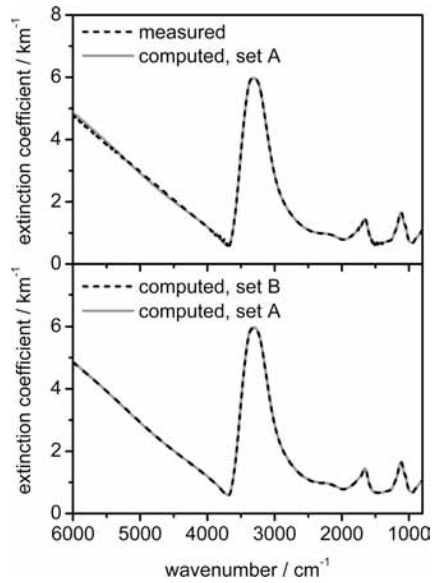

Figure 15. Top panel: measured spectrum at t = 616 s during expansion experiment **A** (20 wt % H_2SO_4, dashed black line) in comparison with the computed spectrum after having optimized the initial guess n and k optical constants with the size distribution parameter set A (N = 16397 cm^{-3}, σ_g = 1.482, and CMD = 0.6327 μm) as input (solid gray line). Bottom panel: comparison of the computed spectrum from the top panel (solid gray line) with another computation using the same n and k values but a different parameter set for the aerosol size distribution (dashed black line; set B with N = 14302 cm^{-3}, σ_g = 1.445, and CMD = 0.6793 μm).

factor of 0.95 to simulate a 5% uncertainty in the H_2SO_4/H_2O mass concentration. The differences between the two retrieval results are similar in magnitude to those between our original n and k data set and the Niedziela et al.[8] n and k spectra shown in Figure 13, leading us to the conclusion that a 5% error in $m_{H_2SO_4/H_2O,0}$ is a reliable estimate for the upper error limit in our measurements.

As the H_2SO_4/H_2O droplet sizes in our experiments are too large to fulfill the conditions of the Rayleigh approximation,[41] the recorded infrared extinction spectra are not directly proportional to the aerosol mass concentration. Instead, the extinction coefficients have to be explicitly calculated with Mie theory for the given aerosol size distribution. In section 3, we have mentioned that the count median diameters of the droplet number size distributions that were directly measured with the DMA system were slightly tuned to bring the results for the integrated size distributions into agreement with our reference values for the H_2SO_4/H_2O mass concentrations from the filter analyses. But instead of modifying the CMD values, we could also have tuned the mode widths of the size distributions or could have scaled the aerosol number concentrations to match the mass loadings from the filter measurements. This would have resulted in modified parameter sets for the H_2SO_4/H_2O aerosol size distributions before the start of pumping which then would have propagated throughout the entire expansion cooling cycles. But the effect on the retrieved n and k data sets of optical constants is negligible because, for droplet sizes below 1 μm, slightly different parameter sets of N, σ_g, and CMD which correspond to the same overall aerosol volume concentration also result in almost the same extinction spectrum.[51] As an example, we consider the measured extinction spectrum from which we have derived the H_2SO_4/H_2O n and k data set for 20 wt % H_2SO_4 at 232 K. The top panel of Figure 15 shows this measured spectrum in comparison with the calculated spectrum after having optimized the initial guess of the optical constants for a size distribution parameter set with N = 16397 cm^{-3}, σ_g = 1.482, and CMD = 0.6327 μm (set A). This parameter set was deduced with the FTIR approach (6000−5000 cm^{-1} spectral fit) using the following start values for the aerosol size distribution at t = 0: N = 18000 cm^{-3}, σ_g = 1.482, and CMD = 0.52 μm. Now let us introduce a modified start parameter set yielding the identical overall aerosol volume concentration, N = 15700 cm^{-3}, σ_g = 1.445, and CMD = 0.56 μm, thereby mimicking the range of uncertainty of the CNC and DMA measurements. As a check, we have then applied the FTIR fit procedure to this modified start parameter set, yielding a droplet size distribution with N = 14302 cm^{-3}, σ_g = 1.445, and CMD = 0.6793 μm (set B) for the extinction spectrum corresponding to 20 wt % H_2SO_4. In the lower panel of Figure 15, we compare the calculated extinction spectrum for the size distribution parameter set A to the spectrum which was computed for the parameter set B using the n and k data set from the iteration with parameter set A.

Both computed infrared spectra are virtually identical (deviations less than 1%). As a practical consequence, an inverse Mie fitting procedure applied to measured infrared extinction spectra of submicron sized aerosol particles will only yield unique retrieval results for the overall aerosol volume concentrations but not for the individual parameters of the size distribution. As to our present study, small uncertainties in the apportionment of the overall H_2SO_4/H_2O mass concentration to a specific parameter set for N, σ_g, and CMD will not affect the retrieval result for the optical constants.

5. Summary

In our present study we have obtained an extension to the database of infrared optical constants in the binary sulfuric acid/water system, addressing for the first time the composition regime involved when supercooled H_2SO_4/H_2O solution droplets enter an environment that is supersaturated with respect to the ice phase at temperatures below 235 K. Prior to the onset of homogeneous ice nucleation, which occurs when the ice saturation ratio has exceeded a temperature-dependent threshold value, the sulfuric acid solution droplets

will continuously dilute by the uptake of water vapor from the gas phase as the ice supersaturation is increased. The atmospheric composition trajectory of sulfuric acid aerosols subjected to a gradually increasing relative humidity was mimicked by slow expansion cooling experiments in the AIDA chamber at initial temperatures of 235, 225, and 211 K. The corresponding composition ranges of the sulfuric acid solution droplets covered by the expansion experiments extended from 33 to 10 wt % H_2SO_4, 36 to 15 wt % H_2SO_4, and 37 to 20 wt % H_2SO_4, respectively.

We have demonstrated that from the interplay of the extensive diagnostic tools of the AIDA chamber these slow expansion cooling cycles could be quantitatively analyzed to yield accurate values for the aerosol composition and mass concentration throughout the entire time period of pumping. On the basis of these input values, the new data sets of infrared optical constants for highly diluted H_2SO_4/H_2O droplets at cirrus temperatures could be deduced using an iterative procedure based on Mie theory calculations. Just as the strong temperature dependency of the optical constants of sulfuric acid aerosols with acid concentrations greater than 37 wt % H_2SO_4, the newly derived data sets for the highly diluted solution droplets also reveal pronounced temperature-induced spectral variations that can be traced back to changes in the equilibrium between sulfate and bisulfate ions. With the help of the new data sets, the homogeneous freezing process of supercooled sulfuric acid solution droplets can be analyzed more accurately with FTIR spectroscopy because it is no longer necessary to employ refractive index data sets that were determined at temperatures well above 235 K to derive the composition of the low-concentrated H_2SO_4/H_2O solution droplets. Though having focused in the present study on the binary sulfuric acid−water system, such expansion cooling experiments could readily be conducted for any kind of supercooled aqueous solution droplets of atmospheric interest.

Acknowledgment. We are grateful for the continuous support by all members of the AIDA staff. We thank two anonymous referees for very careful reading of the manuscript. The work has been funded by the Helmholtz-Gemeinschaft Deutscher Forschungszentren as part of the program "Atmosphere and Climate". Part of this work was also funded within the EU Integrated Project "SCOUT-O3".

Supporting Information Available: Complex refractive indices of H_2SO_4/H_2O from 6000−800 cm^{-1} for selected acid concentrations and temperatures in the regime of 37−10 wt % H_2SO_4 at $T = 235-205$ K. The material is available free of charge via the Internet at http://pubs.acs.org.

References and Notes

(1) Chen, Y. L.; DeMott, P. J.; Kreidenweis, S. M.; Rogers, D. C.; Sherman, D. E. *J. Atmos. Sci.* **2000**, *57*, 3752.

(2) Heymsfield, A. J.; Sabin, R. M. *J. Atmos. Sci.* **1989**, *46*, 2252.

(3) Chang, H. Y. A.; Koop, T.; Molina, L. T.; Molina, M. J. *J. Phys. Chem. A* **1999**, *103*, 2673.

(4) Koop, T.; Ng, H. P.; Molina, L. T.; Molina, M. J. *J. Phys. Chem. A* **1998**, *102*, 8924.

(5) Prenni, A. J.; Wise, M. E.; Brooks, S. D.; Tolbert, M. A. *J. Geophys. Res. (Atmos.)* **2001**, *106*, 3037.

(6) Bertram, A. K.; Patterson, D. D.; Sloan, J. J. *J. Phys. Chem.* **1996**, *100*, 2376.

(7) Cziczo, D. J.; Abbatt, J. P. D. *Geophys. Res. Lett.* **2001**, *28*, 963.

(8) Niedziela, R. F.; Norman, M. L.; DeForest, C. L.; Miller, R. E.; Worsnop, D. R. *J. Phys. Chem. A* **1999**, *103*, 8030.

(9) Myhre, C. E. L.; Christensen, D. H.; Nicolaisen, F. M.; Nielsen, C. J. *J. Phys. Chem. A* **2003**, *107*, 1979.

(10) Tisdale, R. T.; Glandorf, D. L.; Tolbert, M. A.; Toon, O. B. *J. Geophys. Res. (Atmos.)* **1998**, *103*, 25353.

(11) Biermann, U. M.; Luo, B. P.; Peter, T. *J. Phys. Chem. A* **2000**, *104*, 783.

(12) Minogue, N.; Riordan, E.; Sodeau, J. R. *J. Phys. Chem. A* **2003**, *107*, 4436.

(13) Knopf, D. A.; Luo, B. P.; Krieger, U. K.; Koop, T. *J. Phys. Chem. A* **2003**, *107*, 4322.

(14) Koop, T.; Luo, B. P.; Tsias, A.; Peter, T. *Nature* **2000**, *406*, 611.

(15) Carslaw, K. S.; Clegg, S. L.; Brimblecombe, P. *J. Phys. Chem.* **1995**, *99*, 11557.

(16) Wagner, R.; Bunz, H.; Linke, C.; Möhler, O.; Naumann, K. H.; Saathoff, H.; Schnaiter, M.; Schurath, U. "Chamber Simulations of Cloud Chemistry: The AIDA Chamber"; Proceedings of the NATO Advances Research Workshop on Environmental Simulation Chambers: Application to Atmospheric Chemical Processes, held in Zakopane, Poland, from 1 to 4 October 2004, 2006.

(17) Möhler, O.; Stetzer, O.; Schaefers, S.; Linke, C.; Schnaiter, M.; Tiede, R.; Saathoff, H.; Krämer, M.; Mangold, A.; Budz, P.; Zink, P.; Schreiner, J.; Mauersberger, K.; Haag, W.; Kärcher, B.; Schurath, U. *Atmos. Chem. Phys.* **2003**, *3*, 211.

(18) Wagner, R.; Benz, S.; Möhler, O.; Saathoff, H.; Schurath, U. *Atmos. Chem. Phys.* **2006**, *6*, 4775.

(19) Benz, S.; Megahed, K.; Möhler, O.; Saathoff, H.; Wagner, R.; Schurath, U. *J. Photochem. Photobiol. A* **2005**, *176*, 208.

(20) Seifert, M.; Tiede, R.; Schnaiter, M.; Linke, C.; Möhler, O.; Schurath, U.; Ström, J. *J. Aerosol Sci.* **2004**, *35*, 981.

(21) Wagner, R.; Mangold, A.; Möhler, O.; Saathoff, H.; Schnaiter, M.; Schurath, U. *Atmos. Chem. Phys.* **2003**, *3*, 1147.

(22) Ebert, V.; Wolfrum, J. Absorption Spectroscopy In *Optical Measurements - Techniques and Applications*, 2nd corr. ed.; Mayinger, F., Feldmann, O., Eds.; Springer: Heidelberg, München, 2001; pp 227.

(23) Hunsmann, S.; Wunderle, K.; Wagner, S.; Rascher, U.; Schurr, U.; Ebert, V. *Appl. Phys. B: Laser Opt.* **2008**, DOI: 10.1007/s00340−008−3095−2.

(24) Ebert, V. In situ Absorption Spectrometers using Near-IR Diode Lasers and Rugged Multi-Path-Optics For Environmental Field Measurements (paper WB1) In *Laser Applications to Chemical and Environmental Analysis*; OSA Technical Digest (Optical Society of America): Washington, DC, 2006.

(25) Ebert, V.; Teichert, H.; Giesemann, C.; Saathoff, H.; Schurath, U. *Technisches Messen* **2005**, *72*, 23.

(26) Wunderle, K.; Wagner, S.; Pasti, I.; Rascher, U.; Schurr, U.; Ebert, V. 2.7μm DFB Diode Laser Spectrometer for Sensitive Spatially Resolved H_2O Vapour Detection. *Appl. Opt.* Submitted, 2008.

(27) Hunsmann, S.; Wagner, S.; Saathoff, H.; Möhler, O.; Schurath, U.; Ebert, V. Measurement of absorption line strength, pressure broadening coefficients and their temperature dependence for selected lines in the 1.4μm water absorption band In *VDI Berichte 1959*; VDI Verlag: Düsseldorf, 2006; p 149.

(28) Schulz, C.; Dreizler, A.; Ebert, V.; Wolfrum, J. Combustion Diagnostics In *Springer Handbook of Experimental Fluid Dynamics*; Tropea, C., Foss, J., Yarin, A., Eds.; Springer: Berlin, Heidelberg, 2007; p 1241.

(29) Awtry, A. R.; Fisher, B. T.; Moffatt, R. A.; Ebert, V.; Fleming, J. W. *Proc. Comb. Inst.* **2006**, *31*, 799.

(30) Gurlit, W.; Zimmermann, R.; Giesemann, C.; Fernholz, T.; Ebert, V.; Wolfrum, J.; Platt, U.; Burrows, J. P. *Appl. Opt.* **2005**, *44*, 91.

(31) Saathoff, H.; Schiller, C.; Ebert, V.; Fahey, D. W.; Gao, R.-S.; Möhler, O. "The AQUAVIT formal intercomparison of atmospheric water measurement methods"; EGU General Assembly, Geophysical Research Abstracts, EGU2008-A-10485, 2008; Vol. 10, SRef-ID: 1607-7962/gra/EGU2008-A-10485.

(32) Bunz, H.; Benz, S.; Gensch, I.; Krämer, M. *Environ. Res. Lett.* **2008**, *3*, 035001.

(33) Dahneke, B. Simple Kinetic Theory of Brownian Diffusion in Vapors and Aerosols In *Theory of Dispersed Multiphase Flow*; Academic Press: London, 1983.

(34) Carver, R. W.; Harrington, J. Y. "Impact of the mass-accommodation coefficient on cirrus"; 12th Conference on Cloud Physics, 2006, Madison, WI, U.S.A.

(35) Gershenzon, M.; Davidovits, P.; Williams, L. R.; Shi, Q. A.; Jayne, J. T.; Kolb, C. E.; Worsnop, D. R. *J. Phys. Chem. A* **2004**, *108*, 1567.

(36) Murphy, D. M.; Koop, T. *Q. J. R. Meteorol. Soc.* **2005**, *131*, 1539.

(37) Haag, W.; Kärcher, B.; Schaefers, S.; Stetzer, O.; Möhler, O.; Schurath, U.; Krämer, M.; Schiller, C. *Atmos. Chem. Phys.* **2003**, *3*, 195.

(38) Massucci, M.; Clegg, S. L.; Brimblecombe, P. *J. Chem. Eng. Data* **1996**, *41*, 765.

(39) Luo, B.; Krieger, U. K.; Peter, T. *Geophys. Res. Lett.* **1996**, *23*, 3707.

(40) Krieger, U. K.; Mössinger, J. C.; Luo, B. P.; Weers, U.; Peter, T. *Appl. Opt.* **2000**, *39*, 3691.

(41) Bohren, C. F.; Huffman, D. R. *Absorption and Scattering of Light by Small Particles*; John Wiley & Sons, Inc.: New York, 1983.

(42) Norman, M. L.; Qian, J.; Miller, R. E.; Worsnop, D. R. *J. Geophys. Res. (Atmos.)* **1999**, *104*, 30571.

(43) Wagner, R.; Benz, S.; Möhler, O.; Saathoff, H.; Schnaiter, M.; Schurath, U. *J. Phys. Chem. A* **2005**, *109*, 7099.

(44) Press, W. H.; Teukolsky, S. A.; Vetterling, W. T.; Flannery, B. P. *Numerical Recipes in C: The Art of Scientific Computing*; Cambridge University Press: Cambridge, U.K., 1992.

(45) Ohta, K.; Ishida, H. *Appl. Spectrosc.* **1988**, *42*, 952.

(46) Milham, M. E.; Frickel, R. H.; Embury, J. F.; Anderson, D. H. *J. Opt. Soc. Am.* **1981**, *71*, 1099.

(47) Hawranek, J. P.; Neelakantan, P.; Young, R. P.; Jones, R. N. *Spectrochim. Acta, Part A* **1976**, *32*, 85.

(48) Palmer, K. F.; Williams, D. *Appl. Opt.* **1975**, *14*, 208.

(49) Bertie, J. E.; Lan, Z. D. *Appl. Spectrosc.* **1996**, *50*, 1047.

(50) Querry, M. R.; Waring, R. C.; Holland, W. E.; Earls, L. M.; Herrman, M. D.; Nijm, W. P.; Hale, G. M. *J. Opt. Soc. Am.* **1974**, *64*, 39.

(51) Echle, G.; von Clarmann, T.; Oelhaf, H. *J. Geophys. Res. (Atmos.)* **1998**, *103*, 19193.

JP8066102